Erschienen in: Solar Energy Materials and Solar Cells ; 108 (2013). - S. 180-188
https://dx.doi.org/10.1016/j.solmat.2012.09.025

Electrical, optical and structural investigation of plasma-enhanced chemical-vapor-deposited amorphous silicon oxynitride films for solar cell applications

Nils Brinkmann*, Daniel Sommer, Gabriel Micard, Giso Hahn, Barbara Terheiden

University of Konstanz, Department of Physics, P.O. Box X916, 78457 Konstanz, Germany

Keywords:
Surface passivation
Amorphous silicon oxynitride
Wide band gap heterojunctions

A B S T R A C T

Hydrogenated amorphous silicon oxynitride (a-SiO_xN_y:H) films, which are deposited by the plasma decomposition of silane and nitrous oxide at low temperatures ($T_{dep} < 300$ °C), are investigated in order to evaluate the potential of these films for photovoltaic applications. In this work both, intrinsic and doped a-SiO_xN_y:H films are investigated in terms of their electrical, optical and structural properties using Fourier-transform infra-red (FTIR) and secondary-ion mass-spectroscopy (SIMS), as well as high-resolution transmission electron microscopy (HRTEM), photo-conductance decay (PCD), spectral ellipsometry and temperature-dependent conductivity measurements. The plasma deposition parameters are optimized in terms of effective minority carrier lifetime, dark conductivity and low absorbance (i.e. high optical band gap). The optical band gap of the a-SiO_xN_y:H films can be widened up to 2.2 eV compared to a-Si:H due to the incorporation of oxygen and nitrogen into the amorphous network. Not only the optical band gap but also the passivation quality and the dark conductivity of the films are well correlated with the oxygen and nitrogen concentration, which are monitored by means of SIMS measurements. When applying an a-SiO_xN_y:H film with an optical band gap of 2.0 eV, a very high effective minority carrier lifetime of 2.5 ms is measured. In case of doped films, conductivities up to $\sigma_{dark}=4.5\times10^{-3}$ S/cm for the n-type doping and $\sigma_{dark}=3.9\times10^{-4}$ S/cm for the p-type doping are achieved. Combining the intrinsic and doped a-SiO_xN_y:H films to heteroemitter stacks on a crystalline Si base, a very high implied open circuit voltage of up to 733 mV is demonstrated. FTIR and HRTEM measurements reveal a homogenous distribution of Si–Si and Si–O–Si bonds in the a-SiO_xN_y:H films.

1. Introduction

In the ongoing improvement process of crystalline silicon solar cells wafer surface passivation has proven to be a key issue [1]. A high surface recombination velocity directly lowers open circuit voltage and thus cell efficiency [1]. With the production cost driven trend to decrease wafer thickness, surface passivation becomes even more important as the surface-to-volume ratio increases [1].

Intrinsic amorphous silicon (a-Si:H) deposited at low temperatures ($T_{dep} < 250$ °C) by plasma enhanced chemical vapor deposition (PECVD) is reported to provide excellent surface passivation quality [2]. Solar cells with a-Si:H as rear side passivation layer for example yield conversion efficiencies exceeding 20% [3]. Recently, the heterojunction solar cell concept, which employs stacked films composed of an intrinsic passivation and a doped a-Si:H emitter layer, has attracted a lot of attention. Key benefits are the high efficiency potential ($\eta=23.7\%$) and the fact that the whole solar cell process can be carried out at cost and energy efficient temperatures below 200 °C [4,5]. The major drawback of a-Si:H films employed as heteroemitters or passivation layers on the front side of a solar cell is the strong parasitic absorption of light which causes a loss in short circuit current [6]. The absorption within the a-Si:H films can be minimized by widening the optical band gap. This can be realized by the incorporation of for example carbon, nitrogen or oxygen in the amorphous matrix [7].

Si-rich amorphous silicon carbide (a-SiC_x:H) films have been intensively studied and the good passivation quality as well as the doping possibility of these material has been proven [8,9]. But there may still be some more processing difficulties since heterojunction solar cells featuring a-SiC_x:H films as emitter stacks have not yet reached the efficiency of those utilizing pure amorphous silicon [10].

Recently, Mueller et al. [11] studied Si-rich intrinsic amorphous silicon oxide films featuring a very good passivation quality

* Corresponding author. Tel.: +49 7531882088; fax: +49 7531883895.
E-mail addresses: nils.brinkmann@uni-konstanz.de (N. Brinkmann), daniel.sommer@uni-konstanz.de (D. Sommer), gabriel.micard@uni-konstanz.de (G. Micard), giso.hahn@uni-konstanz.de (G. Hahn), barbara.terheiden@uni-konstanz.de (B. Terheiden).

compared to amorphous silicon. Despite the fact that Janotta et al. [16] showed that it is possible to sufficiently dope a-SiO_x:H films, Mueller et al. used only intrinsic a-SiO_x:H but doped a-Si:H films for their heteroemitters [17]. Thus, they do not exploit the full potential of the larger optical band gap of the a-SiO_x:H film.

In this study Si-rich amorphous silicon oxynitride (a-SiO_xN_y:H) films are examined. Silicon oxynitride films have been studied widely for the employment in microelectronics, optics, and mechanics [18–20]. In the field of photovoltaics, only little work has been done, focusing mainly upon the application of intrinsic a-SiO_xN_y:H films as firing stable passivation stacks and as part of an antireflection coating [21,22].

This work, in contrast, focuses on the applicability of a-SiO_xN_y:H films in heterojunction solar cells. Therefore, the structure of a-SiO_xN_y:H films is examined in order to develop films comparable to amorphous silicon in terms of passivation quality and doping efficiency for both n- and p-type doping, but superior to a-Si:H films in terms of light transmittance. The main goal is to develop these films regarding a heteroemitter stack consisting only of a-SiO_xN_y:H films for a considerable improvement in short circuit current density whereas preserving the high open circuit voltage values which are solely possible with a heterojunction solar cell concept.

2. Experimental details

The a-SiO_xN_y:H films are grown by using a commercial PECVD unit (PlasmaLab 100 from Oxford Instruments) in a parallel plate configuration operating with radio frequency (RF) of 13.56 MHz. The decomposition of silane (SiH_4), hydrogen (H_2), and nitrous oxide (N_2O) as precursor gases leads to the desired a-SiO_xN_y:H films. In order to achieve n- or p-type doping of these films phosphine (PH_3) or diborane (B_2H_6) is added to the precursor gases. Both, phosphine and diborane are diluted in hydrogen. All nitrous oxide gas flows quoted in this work refer to their dilution ratio in silane $R_{N_2O}=[N_2O]/([N_2O]+[SiH_4])$. The same is valid for phosphine $R_{PH_3}=[PH_3]/([PH_3]+[SiH_4])$ and diborane $R_{B_2H_6}=[B_2H_6]/([B_2H_6]+[SiH_4])$ gas flows.

The passivation quality of the a-SiO_xN_y:H films is evaluated in terms of the effective minority carrier lifetime τ_{eff} of surface passivated crystalline silicon wafers. Lifetime measurements are conducted on 250 µm thick 2 Ω cm boron-doped high quality float-zone (FZ) silicon wafers (100)-oriented. They are firstly cut by laser in 5×5 cm^2 pieces and are subsequently subjected to a chemical polishing solution in order to remove the laser damage [23]. Secondly, the wafers are cleaned in a standard RCA solution [24]. The RCA oxide is stripped off in a diluted hydrofluoric acid solution (HF, 2%) shortly before the deposition of the a-SiO_xN_y:H films. For lifetime samples a-SiO_xN_y:H films are deposited symmetrically, i.e. the same film on both sides of the wafer. The resulting passivation quality is, as already mentioned, quantified by the effective minority carrier lifetime τ_{eff} of the surface passivated wafer. τ_{eff} is determined as a function of the excess carrier density by means of photoconductance decay (PCD) measurement (WCT 120 from Sinton Consulting Inc.) [25]. The PCD measurement is contactless and therefore induces no damage to the samples. Using τ_{eff} evaluated at an excess carrier density of $\Delta n=1\times10^{15}$ cm^{-3} the surface recombination velocity (S_{eff}) is calculated according to (assuming identical S_{eff} on both sides of the wafer) [26]

$$S_{eff}=\frac{W}{2}\left(\frac{1}{\tau_{eff}}-\frac{1}{\tau_{bulk}}\right) \tag{1}$$

where τ_{bulk} being carrier lifetime in the silicon bulk, and W denoting wafer thickness. For the calculation of S_{eff} infinite bulk lifetime τ_{bulk} is assumed for the float-zone wafers used yielding an upper limit of S_{eff}.

To "activate" the passivation of the a-SiO_xN_y:H films, an annealing step has been proven necessary. This annealing step is carried out on a hotplate in ambient air.

The thickness of the deposited films d_{film} as well as other properties like the refractive index n and the extinction coefficient k are determined by measuring ellipsometry spectra (ψ, Δ) between 250 and 1000 nm. These data are fitted by a Kramers–Kronig-consistent model to extract the quantities to be determined [27]. The optical band gap E_g is calculated from the ellipsometry data by using Tauc's formula [28]

$$\alpha(\hbar\omega)\sim\frac{(\hbar\omega-E_g)^2}{\hbar\omega} \tag{2}$$

with $\alpha=4\pi k/\lambda$.

For conductivity measurements the n- and p-doped a-SiO_xN_y:H films are deposited on borosilicate glass. After the plasma deposition titanium/palladium/silver contacts are applied on top of the (n, p) a-SiO_xN_y:H films by using an electron beam evaporator. The samples are subsequently sintered for 90 min at 150 °C in a nitrogen atmosphere in order to establish the contact between metal and the (n, p) a-SiO_xN_y:H films. Thereupon, lateral conductivity in the dark σ_{dark} as well as the activation energy E_a is determined by temperature dependent measurements of the IV-characteristic of the manufactured samples [29].

A qualitative bonding analysis of the a-SiO_xN_y:H films is performed by means of Fourier-transform infra-red spectroscopy (FTIR) on wafers prepared the same way as for lifetime measurements, but with the films only deposited on one side ($d_{film}>150$ nm) and the other side polished mechanically. The a-SiO_xN_y:H films are measured at room temperature in a nitrogen atmosphere, using a resolution in wavenumbers of 7 cm^{-1}. The effective absorption coefficient is calculated according to [30]

$$\alpha_{eff}=\frac{A_{film}}{d_{film}\log_{10}e} \tag{3}$$

where A_{film} being the absorbance of the a-SiO_xN_y:H films ($A_{film}=A_{sample}-A_{substrate}$). A baseline correction, i.e. a subtraction of the Drude term, is applied to all FTIR data prior to the calculation of the effective absorption coefficient.

Integrating over the absorption band of interest yields the intensity I of this bond [31]:

$$I=\int\frac{\alpha_{eff(\omega)}}{\omega}d\omega \tag{4}$$

This intensity is proportional to the total bond density [31] and is used in this work to qualitatively compare the bond densities in various a-SiO_xN_y:H films.

The absolute concentration of oxygen, nitrogen, boron, and phosphorus atoms within the amorphous network of the a-SiO_xN_y:H films is measured by means of secondary-ion mass spectroscopy (SIMS) [32].

High resolution transmission electron microscopy (HRTEM) images of some selected layers are taken in order to evaluate the structure of the a-SiO_xN_y:H films.

3. Results and discussion

3.1. Intrinsic a-SiO_xN_y:H films

3.1.1. Passivation quality

Independent of the deposition parameters, all c-Si FZ wafers passivated by a-SiO_xN_y:H films (thickness 30 nm) show effective lifetime values which are lower than $\tau_{eff}<100$ µs in the

as-deposited state. However, effective minority carrier lifetime can be increased by subsequent annealing of the samples on a hotplate. An annealing temperature of 300 °C (set temperature) in ambient air results in the optimum surface passivation. Therefore, in the following all reported lifetime values are determined in the annealed state (15 min at 300 °C).

Initially, the a-SiO_xN_y:H films are deposited at various substrate temperatures in the range of 125–325 °C with a N_2O dilution of $R_{N_2O}=16.5\%$. The highest passivation quality is achieved at a deposition temperature of 175 °C yielding $\tau_{eff}=2.45$ ms, which corresponds to $S_{eff}=5.05$ cm/s. This optimum deposition temperature is in the range which was reported for highly passivating a-Si:H and a-SiO_x:H films, too [11,33]. In the following the deposition temperature of all investigated intrinsic a-SiO_xN_y:H films has been set to 175 °C.

In general, the passivation quality of the (i) a-SiO_xN_y:H films enhances with increasing deposition power (Table 1). Therefore, in the following all intrinsic a-SiO_xN_y:H films are deposited at a deposition power of 100 W if not stated otherwise. The growth rate depends inversely on the deposition power and thus decreases with increasing deposition power (Table 1), which is opposed to what is commonly observed for the deposition of a-Si:H and a-SiO_x:H films. The reason might be the use of N_2O as precursor gas, instead of O_2 or CO_2, which dissociates in different species depending on the plasma power.

The pressure influences mainly the growth rate and the homogeneity of film thickness on a large area and is therefore not discussed within this work.

In Fig. 1a the effective lifetime of a-SiO_xN_y:H passivated c-Si FZ wafers is depicted as a function of R_{N_2O} for the high deposition power regime of the PECVD system (100 W). It is observable that effective minority carrier lifetime decreases linearly with increasing N_2O dilution for the examined N_2O dilutions. Without adding N_2O to the precursor gas, an effective lifetime value of 4.3 ms ($S_{eff}=2.9$ cm/s) is achieved (see Fig. 1a). This very high effective lifetime is within the range of values reported for c-Si FZ wafers passivated with amorphous silicon (a-Si:H) films [2]. When applying an (i) a-SiO_xN_y:H film with an optical gap of 2.0 eV ($R_{N_2O}=16.5\%$) as passivation film, a still very high τ_{eff} of 2.45 ms ($S_{eff}=5.05$ cm/s) is determined.

The growth rate increases with increasing N_2O dilution from 5.1 Å/s at $R_{N_2O}=13\%$ to 7.3 Å/s at $R_{N_2O}=31\%$. These growth rates are slightly higher than the rates reported by Mueller et al. [11] for (i) a-SiO_x:H films (1.6–4.1 Å/s).

By comparing qualitatively the shape of the $S_{eff}(\Delta n)$ curves for the samples deposited at different R_{N_2O} (not depicted) it is evident that the passivation mechanism due to field effect is strengthened with increasing R_{N_2O}. Nevertheless, this effect is overcompensated by a strong increase of the dangling bond density at the interface, resulting in a decrease of the minority carrier lifetime with increasing R_{N_2O} (Fig. 1a). The attempt to quantitatively extract the interface defects as well as the fixed charges at the interface from these curves just by adapting the model proposed by Olibet et al. [12], which attributes the recombination at the a-Si:H/c-Si interface totally to a recombination via the amphoteric dangling bond states, has been only successful for Si-rich a-SiO_xN_y:H films ($R_{N_2O}<10\%$). a-SiO_xN_y:H films deposited with $R_{N_2O}>10\%$ could neither be fitted by using the Olibet model nor by using the Shockley–Read–Hall (SRH) recombination model [13,14]. The recombination at the a-SiO_xN_y:H/c-Si interface is therefore most probably a superposition of the recombination via the amphoteric dangling bond states and the SRH-recombination via different defect states.

It is known that the surface passivation quality of a-Si:H is not stable under illumination [15,33]. This light-induced degradation occurs in a-Si:H/c-Si structures by the creation of dangling-bonds [15]. Therefore some lifetime samples were exposed to light (1 sun illumination) for 13.5 h at constant temperature of 50 °C. The light-induced degradation occurs in a-SiO_xN_y:H films in the same way as for a-Si:H films, but is less pronounced with increasing R_{N_2O} (Fig. 1a). However, as it is known for a-Si:H

Table 1
Effective minority carrier lifetime, optical band gap, refractive index and growth rate for a-SiO_xN_y:H films which are deposited in the low (25 W) and high (100 W) power regime at a N_2O dilution of 20% ($T_{dep}=300$ °C).

$R_{N_2O}=20\%$	$P=25$ W	$P=100$ W
τ_{eff} (ms)	0.14	1.94
E_g (eV)	2.2	2.03
n	2.46	3.24
r (Å/s)	8.0	5.7
[O] (cm^{-3})	3×10^{22}	1×10^{22}
[N] (cm^{-3})	2×10^{21}	3×10^{21}

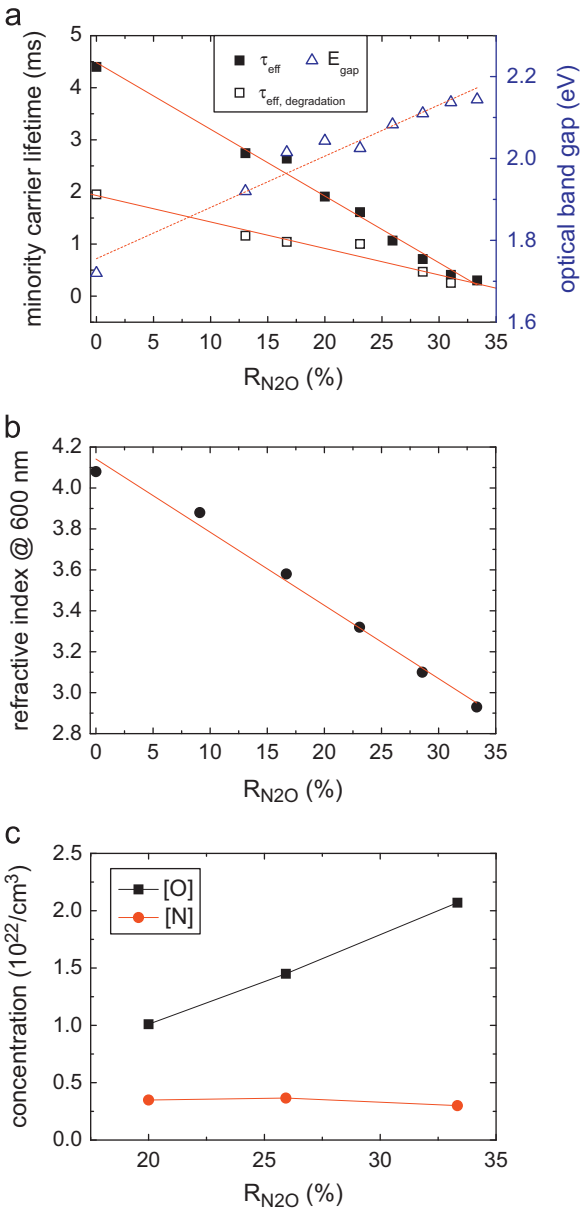

Fig. 1. (a) Effective minority carrier lifetime and optical band gap, (b) refractive index (real part) n, and (c) oxygen and nitrogen concentration of a-SiO_xN_y:H films as a function of N_2O dilution in silane ($T_{dep}=175$ °C, $P=100$ W).

passivated samples, the minority carrier lifetime of a-SiO_xN_y:H passivated samples can almost be recovered by a short annealing step at 300 °C.

3.1.2. Optical band gap

The optical band gap of amorphous silicon strongly depends on its atomic composition [7]. A widening can be achieved e.g. by adding carbon, nitrogen or oxygen into the amorphous matrix [7]. Therefore, it is evident that the optical band gap of the deposited a-SiO_xN_y:H films widens with increasing N_2O gas flow (Fig. 1a). It has to be noticed, that the optical band gap of the a-SiO_xN_y:H films depends linearly on the N_2O dilution in the examined regime as it is also the case for effective lifetime (see Fig. 1a).

The optical band gap of films which are deposited without N_2O in the precursor gas mixture ($R_{N_2O}=0\%$) is determined to be 1.72 eV, which is again in accordance with the values reported in literature for a-Si:H layers [7]. The optical band gap widens to 2.15 eV for films deposited at $R_{N_2O}=35\%$.

Independently from the N_2O dilution, the optical band gap of a-SiO_xN_y:H films increases with decreasing deposition power (Table 1).

The widening of the optical band gap is accompanied by a decrease of the absorption coefficient resulting in a lower absorption within the a-SiO_xN_y:H films over the whole wavelength range compared to amorphous silicon (Fig. 2). This phenomenon renders these films interesting for solar cell application (e.g. as emitter in heterojunction solar cells).

3.1.3. Refractive index

The refractive index n, evaluated at a wavelength of 600 nm, depends on the N_2O dilution and the deposition power in a similar way as the effective minority carrier lifetime. On one hand the refractive index at a wavelength of 600 nm is increasing with increasing deposition power (Table 1). On the other hand the refractive index decreases linearly with increasing N_2O dilution (Fig. 1b) starting at $n=4.08$ for the a-Si:H film ($R_{N_2O}=0\%$). Note that the refractive index of stoichiometeric SiO_2 has been determined to 1.48 [18].

The simple adjustability of the refractive index could make these films interesting for application in multilayer antireflection coatings in particular on the rear side of the solar cell on which absorption within the films does not cause major problems.

3.1.4. Compositional analysis

The concentrations of nitrogen and oxygen in some selected a-SiO_xN_y:H films are determined by means of SIMS measurements (Fig. 1c). The concentration of nitrogen remains almost constant

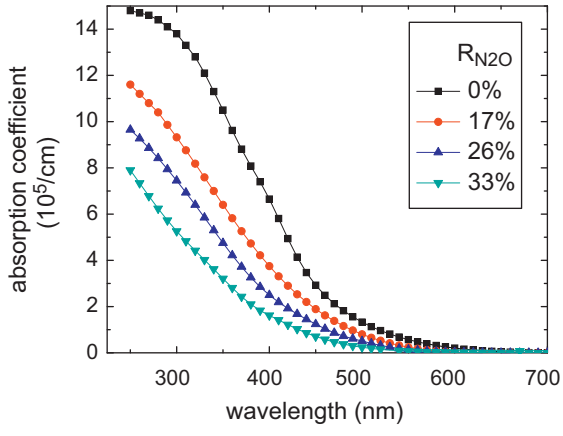

Fig. 2. Spectral absorption coefficient α of a-SiO_xN_y:H films deposited at various N_2O dilutions ($T_{dep}=175$ °C, $P=100$ W).

when increasing the N_2O dilution (at least between $R_{N_2O}=20$–30%), whereas the oxygen concentration increases linearly. This dependence correlates with the linear increase of the optical band gap and the linear decrease of the effective lifetime τ_{eff} (see Fig. 1a). The diminishment of τ_{eff} can be attributed to the increase of the oxygen concentration in the a-SiO_xN_y:H films, which is accompanied by an increase of the bulk defect density [16]. This in turn determines the density of interface traps D_{it} between amorphous and crystalline silicon in the equilibrium state and thus decreases effective minority carrier lifetime [34].

The same argumentation is true to explain the described differences between the low (25 W) and the high power (100 W) regime (see Table 1). In the high power regime, the oxygen concentration in the deposited film ($R_{N_2O}=20\%$, $[O]=1\times10^{22}\,cm^{-3}$) is much lower compared to the low power regime deposited films ($R_{N_2O}=20\%$, $[O]=3\times10^{22}\,cm^{-3}$), yielding a higher effective minority carrier lifetime and a lower optical band gap for the films deposited at high power.

On the contrary, the nitrogen concentration in the a-SiO_xN_y:H films decreases with decreasing power (Table 1). The reason for this different behavior of nitrogen and oxygen is not yet understood and therefore subject to further investigations.

When comparing a-SiO_xN_y:H films with a-SiO_x:H films, which are deposited by adding N_2O or CO_2, respectively, to the precursor gas, some differences are observed. The oxygen concentration in a-SiO_xN_y:H films ($[O]\sim10^{22}\,cm^{-3}$) is in the same order of magnitude as reported for a-SiO_x:H films [11]. The nitrogen concentration in the a-SiO_xN_y:H films, however, is in the order of $[N]\sim10^{21}\,cm^{-3}$ whereas Mueller et al. [11] observed only a carbon concentration in the a-SiO_x:H films which is up to three orders of magnitude lower ($[C]\sim10^{18}$–$10^{19}\,cm^{-3}$). Since the nitrogen concentration of the films investigated in this study is only one order of magnitude lower than the oxygen concentration, it is reasonable to speak of amorphous silicon oxynitride films instead of amorphous silicon oxide films. The reason for the different behavior of nitrogen and carbon needs to be further investigated.

The bonding structure of the a-SiO_xN_y:H films is investigated qualitatively by means of FTIR spectroscopy.

In order to ascertain if the structure of the intrinsic films is changed by the incorporation of boron or phosphorous atoms, both, the intrinsic and the doped films have been deposited in the low power regime (<25 W). However, the doped films are discussed in detail in section 3.2.

An almost linear shift of the center of the Si-O-Si stretching mode peak ($1009\,cm^{-1}$ at $R_{N_2O}=10\%$) toward higher wavenumbers is observable with increasing N_2O dilution ($1020\,cm^{-1}$ at $R_{N_2O}=33\%$) for the intrinsic films (Fig. 3a).

This shift is simply related to the oxygen content in the film [35]. Since the mass of oxygen is approximately equal to one half that of silicon, oxygen and silicon are similarly displaced by the vibrations. Therefore, the vibration frequency depends on the surrounding atoms of the Si–O–Si bond. The frequency of an isolated Si–O–Si bond in an a-Si:H network is $940\,cm^{-1}$, whereas the frequency shifts to $1080\,cm^{-3}$ for a Si–O–Si bond in a-SiO_2 [35].

The linearity of the frequency shift reveals a homogenous distribution of Si–Si and Si–O–Si bonds in the a-SiO_xN_y:H films [19,20]. The assumption of a homogenous distribution is further corroborated by HRTEM measurements (Fig. 4), which do show neither separated phases nor nanoparticles. This finding is in accordance with Scopel et al. [19] who observed a mixture of separated phases only at very high N_2O dilutions ($R_{N_2O}>83\%$).

Beside the peak position shift of the Si–O–Si bond stretching mode, two other peaks located at around $2000\,cm^{-1}$ and $2060\,cm^{-1}$ shift toward higher wavenumbers with increasing N_2O dilution (Fig. 3b).

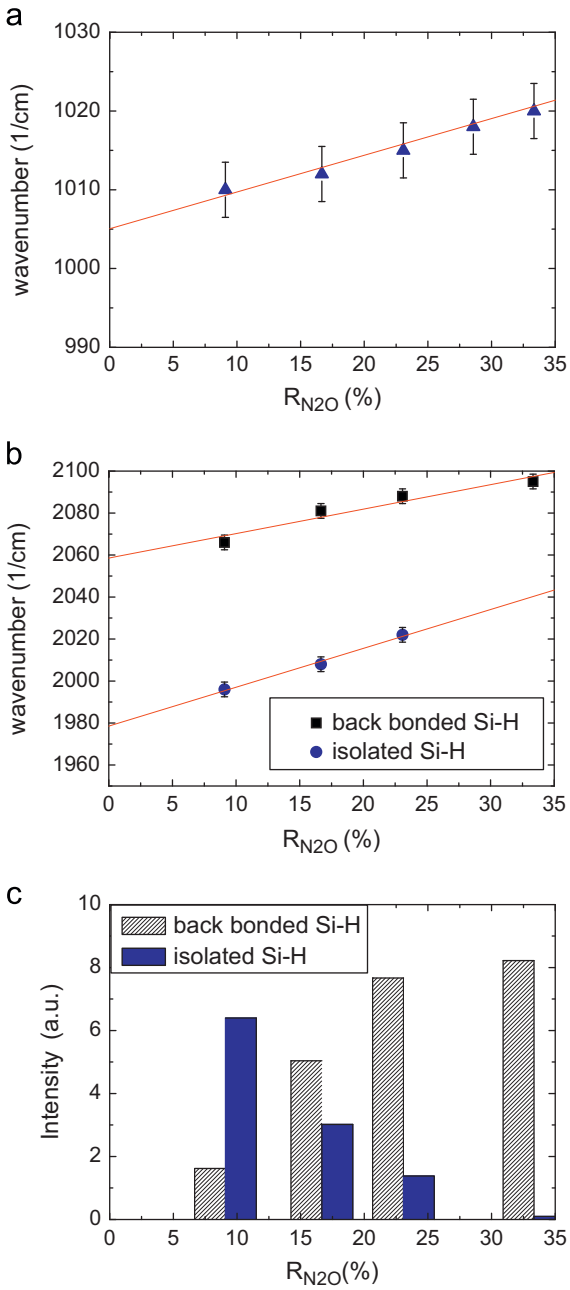

Fig. 3. (a) Peak position of Si–O–Si stretching mode vibrations and (b) of Si–H stretching mode vibrations of a-SiO_xN_y:H films as a function of N_2O dilution determined by means of FTIR measurements (T_{dep}=175 °C, P=5 W). (c) Intensities of the infrared absorption peak of the Si–H bonds, which are isolated, i.e. back bonded only to Si, and back bonded to oxygen in dependence of the N_2O dilution. Note, that the intensity is a proportional for the overall concentration of the bond.

Both peaks originate from Si–H bond stretching vibrations of a monohydride bonding arrangement.

The absorption peak at around 2000 cm^{-1} is caused by Si–H bonds, in which the Si atom has only Si neighbors [31,36], whereas the peak at 2060 cm^{-1} can be attributed to Si–H stretching vibrations, in which one of the atoms back-bonded to the silicon is an oxygen atom [37].

The peak at 2060 cm^{-1} is explained by the higher electro-negativity of the back-bonded oxygen atom compared to the one of a back-bonded Si atom resulting in a partially removal of charge from the Si atom which is bonded to the hydrogen. This yields a reduction of the bonding length, which in turn increases the bonding energy along with the frequency [38].

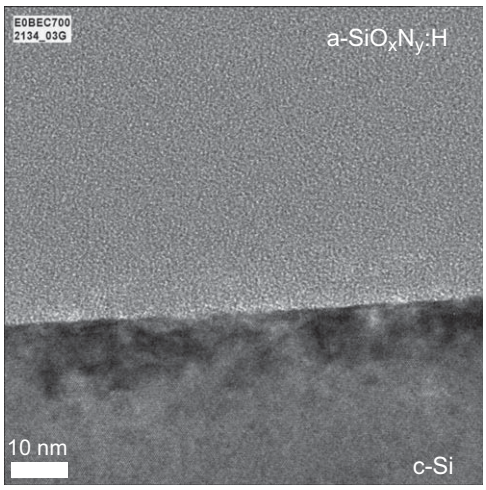

Fig. 4. HRTEM image of an intrinsic a-SiO_xN_y:H film on a c-Si substrate. Neither clusters nor nanoparticles are visible within the a-SiO_xN_y:H film. The dark regions in the c-Si close to the interface might be strains due to plasma damage.

The shift in frequency introduced by a Si–H bond which is back-bonded to nitrogen is only around 24 cm^{-1} [37]. This is within the width of the Si–H bond stretching mode and therefore not clearly observable [37].

The already discussed shift of both peaks toward higher wavenumbers with increasing N_2O dilution originates from an enhanced electro-negativity of the neighbors being more distant from the Si–H bond [37]. Thus, more oxygen atoms are incorporated in the amorphous network with increasing N_2O dilution. Furthermore, the intensity of the isolated Si–H peak decreases with increasing N_2O dilution for the benefit of the intensity of the Si–H peak which is back-bonded to an oxygen atom (Fig. 3c), supporting the finding that more oxygen atoms are incorporated in the a-SiO_xN_y:H film with increasing N_2O dilution. The hydrogen content in the passivating a-SiO_xN_y:H films ranges from 15% to 30%, which is the same order of magnitude as reported for a-Si:H films [34].

There is no evidence in the infrared absorption spectra for O–H groups and N–H groups.

3.2. *Doped a-SiO_xN_y:H films*

In order to manufacture n- and p-doped a-SiO_xN_y:H films, phosphine (PH_3) or diborane (B_2H_6), respectively, diluted in hydrogen is added to the precursor gases. For the phosphorus doped a-SiO_xN_y:H films, dark conductivities up to $\sigma_{dark}=4.5\times10^{-3}$ S/cm (R_{N_2O}=9%) could be reached. The maximum dark conductivity of the boron doped a-SiO_xN_y:H films is one order of magnitude lower ($\sigma_{dark}=3.9\times10^{-4}$ S/cm, R_{N_2O}=9%). These dark conductivities are of the same order as the reported dark conductivities of n- and p-doped a-SiO_x:H [16]. The thickness of the doped a-SiO_xN_y:H films is in the range of 40–60 nm.

3.2.1. *Effect of deposition temperature and power*

The intrinsic a-SiO_xN_y:H films are deposited at a deposition temperature of 175 °C in order to maximize minority carrier lifetime, whereas the deposition temperature of the doped a-SiO_xN_y:H films is set to 300 °C to achieve a higher doping efficiency. Regardless of the fact that doping efficiency is enhanced with increasing temperature, the investigated maximum deposition temperature is 300 °C in order to keep the possibility to apply these films as emitter layers in a low-temperature heterojunction solar cell process.

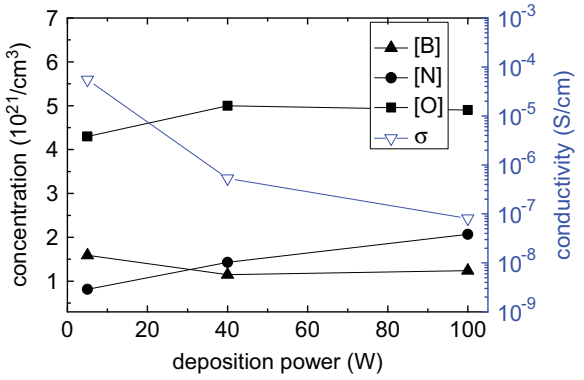

Fig. 5. Boron, nitrogen and oxygen concentration (left axis) and dark conductivity (right axis) of (p) a-SiO_xN_y:H films as a function of deposition power (T_{dep}=300 °C, R_{N_2O}=16.5%, $R_{B_2H_6}$=2.3%).

All doped films are deposited in the low power regime (< 25 W) as opposed to the intrinsic films. Increasing the deposition power as high as for the manufacture of intrinsic films (100 W) yields a reduced conductivity (Fig. 5). This is supposed to be caused by a higher degree of disorder of the film, which arises from an enhanced incorporation of oxygen and nitrogen in the amorphous network (see Fig. 5) as well as from a heightened growth rate with increasing power (r_5 W=2.6 Å/s, r_{100} W=4.8 Å/s). Both effects result in a higher amount of doping atoms being electrically inactive incorporated in the amorphous network [16].

It has to be noticed that the phosphorus films have been deposited at 20 W whereas the boron doped films have been deposited at 5 W in order to attain highest conductivities for both films which is required for high efficiency heteroemitters.

3.2.2. *Effect of N_2O dilution R_{N_2O}*

The conductivity of the n- and p-doped a-SiO_xN_y:H films strongly depends on the optical band gap and thus on the N_2O dilution R_{N_2O}(Fig. 6). Increasing R_{N_2O} results in a higher optical band gap and a lower dark conductivity for both n- and p-type films. The same behavior was reported for amorphous silicon oxide films prepared by using SiH_4 and CO_2 as precursor gases [16].

The reason for the increasing optical band gap with increasing R_{N_2O} is, similarly to the intrinsic a-SiO_xN_y:H film case, a higher concentration of oxygen in the films, as revealed by SIMS measurements (Fig. 7). It is observed that the concentration of oxygen increases with increasing R_{N_2O}, whereas the concentrations of nitrogen, phosphorus, and boron remain almost constant. Despite the incorporation of phosphorus or boron in the film, the dependence of the oxygen and nitrogen concentration from the N_2O dilution is the same as for the intrinsic case (see Fig. 1c). Since the concentration of doping atoms in the film remains constant when increasing R_{N_2O}, the incorporation of these atoms in the amorphous network is not suppressed by oxygen. Hence, the decreasing conductivity of the doped a-SiO_xN_y:H films with increasing R_{N_2O} originates from an enhanced disorder in the films caused by a much higher incorporation of oxygen. It has to be noticed, that the higher the degree of disorder in the amorphous network, the larger the amount of phosphorus/boron atoms which are incorporated electrically inactive [16].

3.2.3. *Effect of phosphine dilution R_{PH_3}*

Increasing the phosphine dilution R_{PH_3} results in a larger phosphorus concentration in the (n) a-SiO_xN_y:H films (Fig. 8). The concentration of oxygen and nitrogen atoms, however,

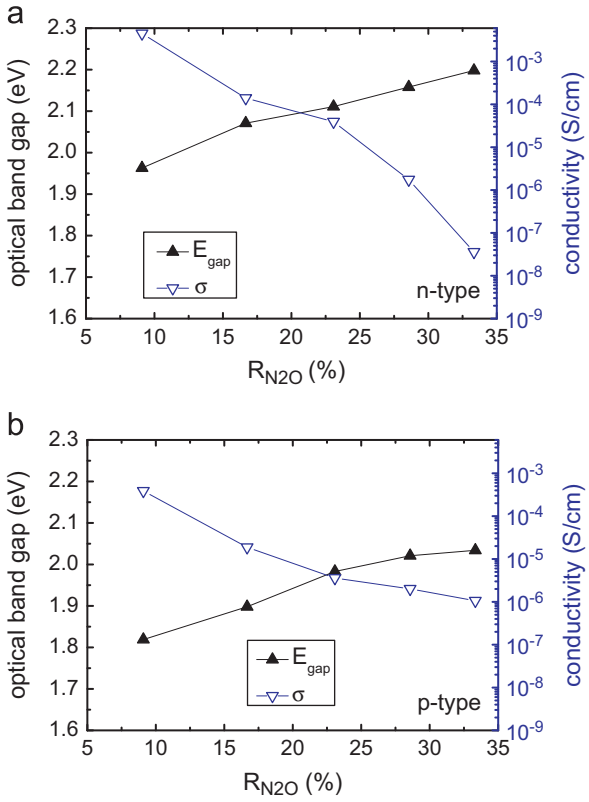

Fig. 6. (a) Optical band gap (left axis) and dark conductivity (right axis) of (n) a-SiO_xN_y:H films and (b) (p) a-SiO_xN_y:H films as a function of N_2O dilution (T_{dep}=300 °C, R_{PH_3}=$R_{B_2H_6}$=2.3%, P_{PH_3}=20 W, and $P_{B_2H_6}$=5 W).

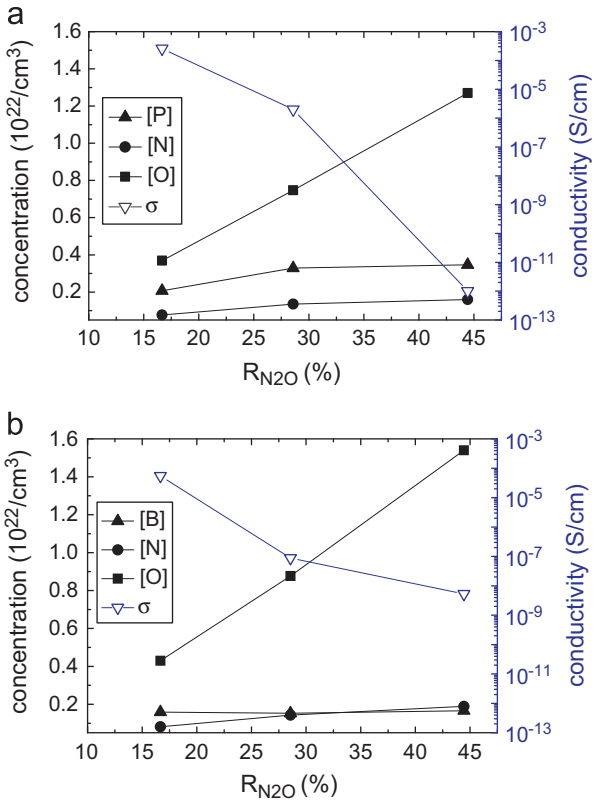

Fig. 7. Phosphorus/boron, nitrogen and oxygen concentration (left axis) and dark conductivity (right axis) of (a) (n) a-SiO_xN_y:H films and (b) (p) a-SiO_xN_y:H films as a function of N_2O dilution (T_{dep}=300 °C, R_{PH_3}=$R_{B_2H_6}$=2.3%, P_{PH_3}=20 W, and $P_{B_2H_6}$=5 W).

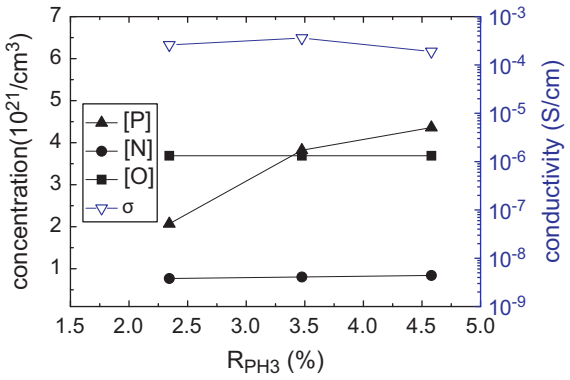

Fig. 8. Phosphorus, nitrogen and oxygen concentration (left axis) and dark conductivity (right axis) of (n) a-SiO_xN_y:H films as a function of PH_3 dilution. (T_{dep}=300 °C, R_{N_2O}=16.5%, and P=20 W).

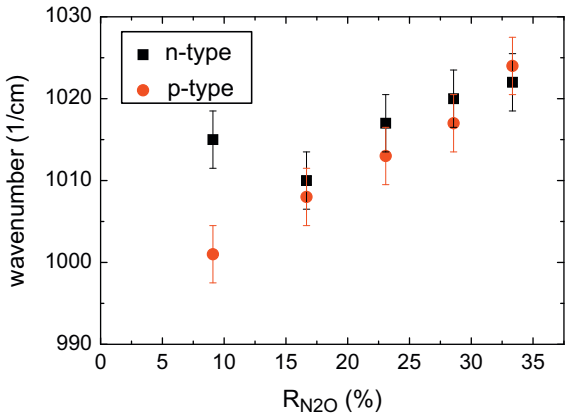

Fig. 9. Peak position of Si–O–Si stretching mode vibrations of phosphorus- (black squares) and boron- doped (red diamonds) a-SiO_xN_y:H films as a function of N_2O dilution determined by means of FTIR measurements (T_{dep}=300 °C, $R_{B_2H_6/PH_3}$=2.3%, and P=5 or 20 W). (For interpretation of the references to color in this figure legend, the reader is referred to the web version of this article).

remains constant. Hence, an enhanced incorporation of phosphorus atoms does not lead to a suppressed incorporation of both oxygen and nitrogen. The dark conductivity does not change much with the R_{PH_3} dilution in the investigated range, meaning that the additional amount of phosphorus is incorporated electrically inactive in the amorphous network. Reducing the phosphine dilution to values less than 2% yields conductivities which are too low for an application of these films as heteroemitters.

The conductivity of boron doped a-SiO_xN_y:H films feature an analog dependency on the diborane dilution as the phosphine doped films (not depicted here).

3.2.4. Activation energy

The activation energy E_a, which is a good approximation of the energy distance between the Fermi energy E_F and the band edges [7], has been determined by temperature dependent conductivity measurements between 175 and 310 K. E_a ranges from 0.14 to 0.39 eV with a very high linearity of the Arrhenius plot for all investigated a-SiO_xN_y:H films and accounts well for the behavior of the observed dark conductivities.

Hence, the activation energy enhances with increasing N_2O dilution from E_a~0.165 eV at R_{N_2O}=16.5% to E_a~0.385 eV at R_{N_2O}=44% for both n- and p-type films and thus reflects the behavior of the conductivity, which decreases with increasing N_2O dilution (see Fig. 7).

Increasing the deposition power results also in an enhancement of E_a which is accompanied by a drop of conductivity ($E_{a,\ 5\ W}$=0.167 eV, $E_{a,\ 100\ W}$=0.274 eV).

Comparing the activation energy and the conductivity depending on the phosphine dilution, both stay constant at around 0.155 eV and 2.76×10^{-4} S/cm, respectively.

Although the conductivities of the a-SiO_xN_y:H films are comparable to the ones reported for doped a-SiO_x:H films by Janotta et al. [16], the activation energies are slightly lower for the a-SiO_xN_y:H films.

3.2.5. FTIR analysis

Similar to the intrinsic a-SiO_xN_y:H films, the peak position of the Si–O–Si bond stretching mode of the doped films shifts linearly toward higher wavenumbers with increasing R_{N_2O}. The only difference is that the linear shift of the doped films starts at smaller wavenumbers (Fig. 9). This is most probably caused by a different average electro-negativity of the host matrix. The linearity of the shift originates from the homogenous distribution of Si–Si and Si–O–Si bonds within the doped films [19,20]. This homogenous distribution is further confirmed by HRTEM imaging (not displayed here).

The structure of the a-SiO_xN_y:H films is therefore not altered by the incorporation of boron and phosphorus atoms.

3.3. Employment as heteroemitter

In order to employ the investigated a-SiO_xN_y:H films in an emitter stack in heterojunction solar cells, the intrinsic and doped films are combined. These heteroemitter stacks are deposited on both sides of 2 Ω cm p-type c-Si FZ wafers and the structure is evaluated in terms of the implied open circuit voltage (*impl.* V_{oc}) [39].

A very high *impl.* V_{oc} value of up to 733 mV (τ_{eff}=2.35 ms) is achieved for the n-type emitter stack (intrinsic: R_{N_2O}=16.5%, T_{dep}=175 °C, P=100 W; n-doped: R_{N_2O}=16.5%, R_{PH_3}=2.3%, T_{dep}=300 °C, P=20 W). It has to be noticed that, with the utilized PECVD system, the thickness of the intrinsic layers employed in the emitter stacks is limited to a minimum value of around 10 nm and therefore slightly too thick for manufacturing high efficiency heterojunction solar cells. The thickness limitation arises from a fix but to small distance between the two electrodes of the utilized PECVD system.

Due to the relatively thick intrinsic buffer layer (10 nm) no gain in minority carrier lifetime caused by the field effect passivation mechanism, which is introduced by the additional doped emitter layer as reported by De Wolf and Kondo [40], has been observed in this work. The measured minority carrier lifetime of the samples passivated by the emitter stack is therefore, within the measurement uncertainty, the same as for the samples which are passivated only by the corresponding intrinsic layer.

In order to evaluate if the use of a-SiO_xN_y:H instead of a-Si:H as heteroemitter films yields an efficiency gain on solar cell level, the loss in short circuit density due to parasitic absorption within the films has been calculated by using Sunrays [41]. The simulated structure consists of a random pyramid texture, a 15 nm thick stack of intrinsic (5 nm) and doped (10 nm) amorphous films covered by an 80 nm thick layer of a conventional ITO. The same n and k values are assumed for the intrinsic and doped amorphous layers, but taking into account that according to Holman et al. [42] the collection efficiency of carriers generated in the ITO and the doped amorphous films is zero, but 30% of the light absorbed in the intrinsic film contributes to the short circuit current density. The calculated gain of short circuit current density in comparison to the application of amorphous silicon amounts to 1.15 mA/cm^2 for the a-SiO_xN_y:H film deposited with

$R_{N_2O}=17\%$ and 1.85 mA/cm^2 for the film deposited with $R_{N_2O}=26\%$ and $R_{N_2O}=33\%$. Despite of a higher optical band gap of the a-SiO$_x$N$_y$:H film deposited at $R_{N_2O}=33\%$ (Fig. 1a), the gain in short circuit current density is the same as for the film deposited at $R_{N_2O}=26\%$. The reason for the comparable gain is an enhanced reflection at the a-SiO$_x$N$_y$:H/c-Si interface due to a decreasing refractive index n with increasing R_{N_2O} (Fig. 1b).

However, using a-SiO$_x$N$_y$:H instead of a-Si:H layers leads to an increased short circuit current density, but on the other hand the lifetime is decreasing with increasing R_{N_2O} (Fig. 1a) which could raise questions if this is negatively influencing the open circuit voltage of the solar cell. AFORS-HET simulations performed by Conrad et al. [43] have shown that the open circuit voltage of heterojunction solar cell starts to decrease at an interface defect density D_{it} higher than 3×10^{10} cm^{-2} eV^{-1}. According to Plagwitz [6], who reported a D_{it} value of 2×10^{9} cm^{-2} eV^{-1} for amorphous silicon films which yield a surface recombination velocity of 18 cm/s, we do not expect a large loss in open circuit voltage by increasing the R_{N_2O} ratio up to 26%, since the measured effective surface recombination velocity stays below 11 cm/s.

Changing the a-Si:H emitter to an a-SiO$_x$N$_y$:H emitter may result in a drop in fill factor due to the low conductivity of the a-SiO$_x$N$_y$:H, which might counterbalance the gain in short circuit current density. However, Munoz et al. [44] demonstrated experimentally that the fill factor of heterojunction solar cells is not influenced if the conductivity of the doped emitter layer is higher than 1×10^{-5} S/cm. Therefore, we expect a gain in efficiency for the a-SiO$_x$N$_y$:H emitters deposited with $R_{N_2O}<20\%$ compared to the conventional a-Si:H emitter. The gain in short circuit current density for a-SiO$_x$N$_y$:H emitters deposited with $R_{N_2O}>20\%$ can be fully turned into efficiency enhancement if the conductivity of these films is further increased.

4. Conclusion

We studied the applicability of low temperature ($T_{dep}<300$ °C) Si-rich amorphous silicon oxynitride (a-SiO$_x$N$_y$:H) films for crystalline silicon solar cells. The passivation quality as well as the doping efficiency of the (n, p) a-SiO$_x$N$_y$:H films grown by plasma decomposition (PECVD) of silane and nitrous oxide were investigated.

We showed that not only the optical band gap but also the passivation quality and the doping efficiency of the films are well correlated with the oxygen concentration. The latter in turn strongly depends on the deposition parameters. Both minority carrier lifetime and optical band gap depend linearly on the N_2O dilution, but inversely to each other.

In order to maximize effective minority carrier lifetime, a deposition temperature of 175 °C and a high deposition power (100 W) revealed to be the optimum parameter if a post-deposition annealing step at 300 °C follows. When applying an (i) a-SiO$_x$N$_y$:H film with an optical gap of 2.0 eV to a 2 Ω cm p-type FZ wafer (250 μm thick), a very low effective surface recombination velocity of 5 cm/s ($\tau_{eff}=2.5$ ms) was measured.

In case of doped films, conductivities up to $\sigma_{dark}=4.5\times10^{-3}$ S/cm ($R_{N_2O}=9\%$, $E_{gap}=1.97$ eV) for the n-type doping and $\sigma_{dark}=3.9\times10^{-4}$ S/cm ($R_{N_2O}=9\%$, $E_{gap}=1.82$ eV) for the p-type doping were achieved. These high conductivities are in the same order reported for a-Si:H films. However, their higher optical band gaps could lead to a superiority of a-SiO$_x$N$_y$:H films compared to a-Si:H films, as they cause less parasitic absorption of incoming light.

The conductivity of the films decreases with increasing N_2O dilution. This effect is caused by an enhanced incorporation of oxygen resulting in more doping atoms being incorporated electrically inactive. The overall concentration of doping atoms in the film is unaffected by the increase of the oxygen concentration in the films. An optimum doping efficiency was achieved at a higher deposition temperature (300 °C) and at a lower deposition power (20 W for n-type and 5 W for p-type films) compared to the intrinsic films.

FTIR and HRTEM measurements reveal a homogenous distribution of Si–Si and Si–O–Si bonds in the a-SiO$_x$N$_y$:H films. This structure is not altered by the incorporation of boron and phosphorus atoms in the amorphous network.

Combining the intrinsic and doped a-SiO$_x$N$_y$:H films to heteroemitter stacks, a very high implied open circuit voltage of up to 733 mV on a 2 Ω cm p-type FZ-Si wafer was demonstrated. Simulations revealed a short circuit current density gain of up to 1.85 mA/cm^2. This gain can be fully turned into efficiency enhancement if more conductive a-SiO$_x$N$_y$:H films are applied.

In general, the manufacturing of Si-rich a-SiO$_x$N$_y$:H films is similar to the one of amorphous silicon films, i.e. grown by low temperature PECVD. Effective minority carrier lifetimes and conductivities of a-SiO$_x$N$_y$:H films are comparable to a-Si:H films but the first films suffer less from parasitic absorption over the whole wavelength range because of their higher optical band gaps. This fact and the possibility to tune the refractive index in a certain range, turns a-SiO$_x$N$_y$:H into a very interesting material for solar cell applications, especially for heterojunction solar cells and multilayer anti reflection coatings.

Acknowledgments

We would like to thank A. Herguth for fruitful discussions as well as S. Wilking and B. Rettenmaier for technical support. N. Brinkmann gratefully acknowledges the sponsorship by the scholarship program of the German Federal Environmental Foundation (Deutsche Bundesstiftung Umwelt, DBU). The financial support from the BMU project FKZ 0325079 is gratefully acknowledged in particular for the processing equipment.

References

[1] A. Aberle, Crystalline Silicon Solar Cells—Advanced Surface Passivation and Analysis, UNSW, Sydney, 1999, p. 13–46.
[2] S. Dauwe, J. Schmidt, R. Hezel, Very low surface recombination velocities on p- and n-type silicon wafers passivated with hydrogenated amorphous silicon films, in: Proceedings of the 29th IEEE PVSC, 2002, p. 1246.
[3] M. Schaper, J. Schmidt, H. Plagwitz, R. Brendel, 20.1%-efficient crystalline silicon solar cell with amorphous silicon rear-surface passivation, Progress in Photovoltaics: Research and Applications 13 (2005) 381–386.
[4] T. Kinoshita, D. Fujishima, A. Yano, A. Ogane, S. Tohoda, K. Matsuyama, Y. Nakamura, N. Tokuoka, H. Kanno, H. Sakata, M. Taguchi, E. Maruyama, The approaches for high efficiency HITTM solar cell with very thin (<100 μm) silicon wafer over 23%, in: Proceedings of the 26th EUPVSEC, 2011, p. 871.
[5] S. Taira, Y. Yoshimine, T. Baba, M. Taguchi, H. Kanno, T. Kinoshita, H. Sakata, E. Maruyama, M. Tanaka, Our approaches for achieving HIT solar cells with more than 23% efficiency, in: Proceedings of the 22nd EUPVSEC, 2007, p. 932.
[6] H. Plagwitz, Surface Passivation of Crystalline Silicon Solar Cells by Amorphous Silicon Films, Ph.D. Thesis, G.W. Leibniz University of Hannover, 2007.
[7] R.A. Street, Hydrogenerated Amorphous Silicon, Cambridge University Press, Cambridge, 1990, p. 83–88.
[8] S. Janz, Amorphous Silicon Carbide for Photovoltaic Applications, Ph.D. Thesis, University of Konstanz, 2006.
[9] F. Demichelis, C.F. Pirri, E. Tresso, G. Della Mea, V. Rigato, P. Rava, Physical properties of undoped and doped hydrogenated amorphous silicon carbide, Semiconductor Science and Technology 6 (1991) 1141–1146.
[10] D. Pysch, M. Bivour, M. Hermle, S.W. Glunz, Amorphous silicon carbide heterojunction solar cells on p-type substrates, Thin Solid Films 519 (2011) 2550–2554.
[11] T. Mueller, S. Schwertheim, W.R. Fahrner, Crystalline silicon surface passivation by high-frequency plasma-enhanced chemical-vapor-deposited nanocomposite silicon suboxides for solar cell applications, Journal of Applied Physics 107 (2010) 014504-1–014504-11.
[12] S. Olibet, E. Vallat-Sauvain, C. Ballif, Model for a-Si:H/c-Si interface recombination based on the amphoteric nature of silicon dangling bonds, Physical Review B 76 (2007) 035326-1–035326-14.

[13] W. Shockley, W.T. Read, Statistics of the recombinations of holes and electrons, Physical Review 87 (1952) 835–842.
[14] R.N. Hall, Electron–hole recombination in germanium, Physical Review 87 (1952) 387.
[15] H. Plagwitz, B. Terheiden, R. Brendel, Staebler–Wronski like formation of defects at the amorphous-silicon–crystalline silicon interface during illumination, Journal of Applied Physics 103 (2008) 094506-1–094506-4.
[16] A. Janotta, R. Janssen, M. Schmidt, T. Graf, M. Stutzmann, L. Goergens, A. Bergmaier, G. Dollinger, C. Hammerl, S. Schreiber, B. Stitzker, Doping and its efficiency in a-SiO_x:H, Physical Review B 69 (2004) 115206-1–115206-16.
[17] T. Mueller, S. Schwertheim, K. Meusinger, B. Wdowiak, R. Klimkeit, W.R. Fahrner, Application of plasma deposited nanocomposite silicon suboxides and microcrystalline silicon alloys to heterojunction solar cells, in: Proceedings of the 34th IEEE-PVSC, 2009, p. 2378.
[18] M.I. Alayo, I. Pereya, W.L. Scopel, M.C.A. Fantini, On the nitrogen and oxygen incorporation in plasma-enhanced chemical vapor deposition (PECVD) SiO_xN_y films, Thin Solid Films 402 (2002) 154–161.
[19] W.L. Scopel, R.R. Cuzinatto, M.H. Tabacniks, M.C.A. Fantini, M.I. Alayo, I. Pereyra, Chemical and morphological properties of amorphous silicon oxynitride films deposited by plasma enhanced chemical vapor deposition, Journal of Non-Crystalline Solids 288 (2001) 88–95.
[20] K. Haga, H. Watanabe, A structural interpretation of Si–O–Si vibrational absorption of high-photoconductive amorphous a-SiO_x:H films, Journal of Non-Crystalline Solids 195 (1996) 72–75.
[21] A. Laades, M. Blech, H.C. Biank, C. Maier, M. Roczen, C. Leschinski, H. Strutzberg, A. Lawrenz, Fundamental study of silicon oxynitrides for photovoltaic applications, in: Proceedings of the 26th EUPVSEC, 2011, p. 1653.
[22] M. Junghänel, M. Schädel, L. Stolze, S. Peters, Black multicrystalline solar modules using novel multilayer antireflection stacks, in: Proceedings of the 5th WCPEC, 2010, p. 2637.
[23] F.A. Bogenschuezt, Aetzpraxis fuer Halbleiter, Hanser, München, 1967, p. 67–68.
[24] W. Kern, The evolution of silicon wafer cleaning technology, Journal of the Electrochemical Society 137 (1990) 1892.
[25] R.A. Sinton, A. Cuevas, Contactless determination of current–voltage characteristics and minority-carrier lifetimes in semiconductors from quasi-steady-state photoconductance data, Applied Physics Letters 69 (1996) 2510–2512.
[26] A.B. Sproul, Dimensionless solution of the equation describing the effect of surface recombination on carrier decay in semiconductors, Journal of Applied Physics 76 (1994) 2851–2854.
[27] M. Fox, Optical Properties of Solids, Oxford University Press, Oxford, 2010, p. 44–46.
[28] J. Tauc, A. Menth, States in the gap, Journal of Non-Crystalline Solids 8 (1972) 569–585.
[29] Y. Lubianiker, I. Balberg, Two Meyer–Neldel rules in porous silicon, Physical Review Letters 78 (1997) 2433–2436.
[30] D. Suwito, Intrinsic and Doped Amorphous Silicon Carbide Films for the Surface Passivation of Silicon Solar Cells, Ph.D. Thesis, University of Konstanz, 2011.
[31] A.A. Langford, M.L. Fleet, B.P. Nelson, W.A. Landford, N. Maley, Infrared absorption strength and hydrogen content of hydrogenated amorphous silicon, Physical Review B 45 (1992) 13367–13377.
[32] D. Schroder, Semiconductor Material and Device Characterization, John Wiley and Sons, Hoboken, New Jersey, 2006, p. 102–103.
[33] S. De Wolf, B. Demaurex, A. Descoeudres, C. Ballif, Very fast light-induced degradation of a-Si:H/c-Si(100) interfaces, Physical Review B 83 (2011) 233301–233304.
[34] T.F. Schulze, H.N. Beushausen, C. Leendertz, A. Dobrich, B. Rech, Interplay of amorphous silicon disorder and hydrogen content with interface defects in amorphous/crystalline silicon heterojunctions, Applied Physics Letters 96 (2010) 252102–252103.
[35] G. Lucovsky, J. Yang, S.S. Chao, J.E. Tyler, W. Czubatyj, Oxygen-bonding environments in glow-discharge-deposited amorphous silicon–hydrogen alloy films, Physical Review B 28 (1983) 3225–3233.
[36] D.V. Tsu, G. Lucovsky, B.N. Davidson, Effects of the nearest neighbors and the alloy matrix on SiH stretching vibrations in the amorphous SiO_r:H ($0 < r < 2$) alloy system, Physical Review B 40 (1989) 1795–1805.
[37] G.N. Parsons, G. Lucovsky, Silicon–hydrogen bond-stretching vibrations in hydrogenated amorphous silicon–nitrogen alloys, Physical Review B 41 (1990) 1664–1667.
[38] G. Lucovsky, Z. Jing, P. Santos-Filho, G. Stevens, A. Banerjee, Nearest-neighbor repulsion-perturbed silicon monohydride bond-stretching vibrations in hydrogenated and deuterated silicon nitrogen alloy films, Journal of Non-Crystalline Solids 198 (1996) 19–23.
[39] A. Cuevas, R.A. Sinton, Prediction of the open-circuit voltage of solar cells from the steady-state photoconductance, Progress in Photovoltaics: Research Applications 5 (1997) 79–90.
[40] S. De Wolf, M. Kondo, Nature of doped a-Si:H/c-Si interface recombination, Journal of Applied Physics 105 (2009) 103707-1–103707-6.
[41] R. Brendel, SUNRAYS: a versatile ray tracing program for the photovoltaic community, in: Proceedings of the 12th EUPVSEC, 1994, p. 1339.
[42] Z.C. Holman, A. Descoeudres, L. Barraud, F.Z. Fernandez, J.P. Seif, S. De Wolf, C. Ballif, Current losses at the front of silicon heterojunction solar cells, IEEE Journal of Photovoltaics 2 (2012) 7–15.
[43] E. Conrad, L. Korte, K. von Maydell, H. Angermann, C. Schubert, R. Stangl, M. Schmidt, Development and optimization of a-Si:H/c-Si heterojunction solar cells completely processed at low temperatures, in: Proceedings of the 21st EUPVSEC, 2006, p. 784.
[44] D. Munoz, P.J. Ribeyron, A.S. Ozanne, A. Danel, S. Harrison, N. Nguyen, C. Arnal, S. Martin de Nicolas, F. Souche, G. D'Alonzo, T. Desrues, High efficiency a-Si:H/c-Si heterojunction solar cells development at INES, in: Proceedings of the 1st nPV Workshop. 2011.